frontiers | Frontiers in Earth Science

TYPE Original Research
PUBLISHED 15 May 2024
DOI 10.3389/feart.2024.1360202

OPEN ACCESS

EDITED BY
Wenlong Ding,
China University of Geosciences, China

REVIEWED BY
Hu Li,
Southwest Petroleum University, China
Hao Xu,
Chengdu University of Technology, China
Lei Gong,
Northeast Petroleum University, China

*CORRESPONDENCE
Weiming Yu,
wooyu0717@163.com

RECEIVED 22 December 2023
ACCEPTED 26 April 2024
PUBLISHED 15 May 2024

CITATION
Yu W, Yuan S, Tang H, Luo C, Wu W, Liu J, Yang Y, Zhong K and He L (2024), The effect of structural preservation conditions on pore structure of marine shale reservoir: a case study of the Wufeng-Longmaxi Formation shale, Southern Sichuan Basin, China. *Front. Earth Sci.* 12:1360202. doi: 10.3389/feart.2024.1360202

The effect of structural preservation conditions on pore structure of marine shale reservoir: a case study of the Wufeng-Longmaxi Formation shale, Southern Sichuan Basin, China

Weiming Yu[1,2]*, Shusheng Yuan[1,2], Haoxuan Tang[2,3], Chao Luo[1,2], Wei Wu[1,2], Jia Liu[1,2], Yuran Yang[1,2], Kesu Zhong[1,2] and Liang He[1,2]

[1]Shale Gas Research Institute, PetroChina Southwest Oil and Gasfield Company, Chengdu, China, [2]Sichuan Collaborative Innovation Center for Shale Gas Resources and Environment, Chengdu, China, [3]School of Geoscience and Technology, Southwest Petroleum University, Chengdu, China

The marine shale within the Sichuan Basin constitutes China's significant shale gas production, featuring old formation age, high degree of thermal evolution, multiple tectonic movements, and complex structural conditions. However, there are significant differences in the shale gas preservation conditions and reservoir quality in different areas, limiting future large-scale exploration and development. Pore structure significantly influences shale reservoir quality, gas content, and exploration of shale gas occurrence, migration, and enrichment mechanisms. The influence of structural-dominated preservation conditions on shale pore structures is essential to comprehend for effective shale gas exploitation. This study employs field-emission scanning electron microscopy in conjunction with other techniques (low-temperature N_2 adsorption, low-temperature CO_2 adsorption, and nuclear magnetic resonance) for detailed analyses of the pore structure across varied structural zones, revealing the influence of structural attributes, fault systems, depth of burial, and formation pressure on pore architecture, and examining the relationship between pore structure and shale gas preservation conditions. The results show that stable structural condition is conducive to the development and preservation of shale pores. Structural compression causes inorganic and organic pores to become narrow and elongated due to shrinkage, with a significant increase in microfractures. The porosity of shale with stable structural conditions exhibits markedly increased porosity compared to samples under structural compressions. Under conditions of similar TOC and mineral composition, the pore size distribution (PSD), pore volume (PV), and specific surface area (SSA) of shale after structural compression are significantly lower than those of samples with stable structural conditions. As the burial depth increases, the shale porosity shows a decreasing trend, but the decrease is limited. Burial depth significantly impacts the SSA and PV of high-TOC samples (3%–6%). As the burial depth increases, both SSA and PV show a significant decreasing trend. When the burial depth reaches 4000 m, SSA and PV tend

to concentrate. The formation pressure coefficient is an important factor for the development and preservation of shale pores, and porosity is positively correlated with the formation pressure coefficient. Increased formation pressure coefficient indicates superior preservation conditions and enhanced pore development.

KEYWORDS

Wufeng-Longmaxi Formation, marine shale, structural preservation, pore structure, burial depth, Sichuan Basin

Introduction

From the Late Ordovician through Early Silurian (Zou et al., 2016a; Jiang et al., 2017), the Southern Sichuan Basin marked a deep-water continental shelf environment characterized by similar organic-rich marine shale gas enrichment conditions as the North American Craton (Hao et al., 2013; Zou et al., 2016b). It is currently the main contributor to China's shale gas production capacity (Jiang et al., 2016; Dong et al., 2022). Although national shale gas demonstration areas such as Jiaoshiba, Weiyuan, and Changning-Zhaotong have been built (Liang et al., 2021), the next stage of large-scale exploration and development is clearly constrained by current exploration results. Due to the strong compression, uplift, and superimposed deformation of multiple tectonic movements such as the Indosinian, Yanshanian, and Himalayan periods, the folding, faulting, uplift, and erosion in the basin are strong (Hu et al., 2017; Gao et al., 2020; Guo et al., 2021). There are significant differences in reservoir quality and shale gas preservation conditions in different areas (Guo, 2016; Zhu et al., 2021a), which pose significant challenges for the next large-scale exploration and exploitation.

It is now commonly accepted that pore structure plays a important role in reservoir quality, gas content calculation, occurrence mechanism, and enrichment mechanism (Jiang et al., 2019; Yu and Tang, 2019; Fu et al., 2021). It is also the subject of increased research attention on shale oil and gas reservoirs (Fu et al., 2019; Liu et al., 2020; Cai et al., 2023). Previous studies have shown that organic-rich marine shale contains abundant micro and nano-scale pores and a small number of microfractures, making it a reservoir and migration channel for shale gas (Loucks et al., 2012; Klaver et al., 2015; Ko et al., 2018). The pore structure of shale is influenced by internal conditions such as organic matter content, organic matter type, organic-inorganic diagenesis, mineral composition (Chalmers et al., 2012; Milliken et al., 2013; Liu et al., 2020), as well as external factors such as structural feature, fault system, burial depth, etc (Tang et al., 2015; Tang et al., 2022). Most reports have discussed changes in pore structure from the perspectives of mineral composition and organic geochemical indicators (Wang et al., 2022; Zhou et al., 2023). There are also studies discussing the evolution of pore structure from the perspective of organic matter evolution (Pommer and Milliken, 2015; Zhang et al., 2021). Although some reports have noticed that the differences in pore structure reflect the different preservation conditions of shale gas, most of them analyze the preservation modes of shale gas from macro perspectives such as structural styles (Liang et al., 2021; Ma et al., 2023), and there are few studies on the control of micro-scale and nano-scale structures by structural preservation conditions (Liu et al., 2020; Yang et al., 2022). Many authors have addressed the contribution of natural fractures in unconventional reservoirs (Zeng et al., 2022; Gong et al., 2023; Zeng et al., 2023). Natural fracture system plays a key role in the enrichment and high production of shale reservoirs, and studies pointed out that tectonic fractures are the most common fractures influencing to unconventional gas reservoir production (Gong et al., 2023; Zeng et al., 2023). The effect of structural preservation conditions on shale pore structure remain poorly understood compared to current understanding of nanoscale preservation conditions. Establishing the relationship between preservation conditions and pore structure has important scientific significance and exploration practical value for the study of shale gas preservation conditions and the evolution of shale pore structure.

Field emission-Scanning electron microscopy (FE-SEM), low-temperature CO_2 adsorption (LTCA), low-temperature N_2 adsorption (LTNA), and nuclear magnetic resonance (NMR) have been widely used to illustrate pore structure parameters and their controlling factors. Based on comprehensive data of marine shale reservoir in Southern Sichuan Basin, these methods are employed in this study to (i) demonstrate the pore structure of the different structural area, (ii) reveal the effect of structure fault on pore structure, and (iii) quantitatively discuss the correlation between pore structure and structural preservation conditions of shale reservoir.

Geological setting

The study area is located in the southern part of the Sichuan Basin (Figure 1A), with complex structural conditions (Figure 1B). A series of northeast southwest trending anticlines and a series of wide and gentle synclines with the same strike are developed. The studied shale samples are from the Wufeng-Longmaxi Formation in the Western Chongqing, Weiyuan, and Luzhou areas of the Sichuan Basin, which is the main target interval for shale gas exploration and development (Zhu et al., 2021b). Affected by different tectonic processes (Li et al., 2019), heterogeneity was documented in the burial depths of Wufeng-Longmaxi shale in the three areas of Zhaotong (<2000 m), Weiyuan (2,000–3,500 m), and Luzhou (>3,500 m) (Chen et al., 2022). Different stages of tectonic movements greatly controlled the development and preservation of shale gas reservoirs (Xiang et al., 2022), leading to significant differences in shale gas reservoirs in different structural areas and backgrounds (Luo et al., 2022). The quality of shale gas reservoirs

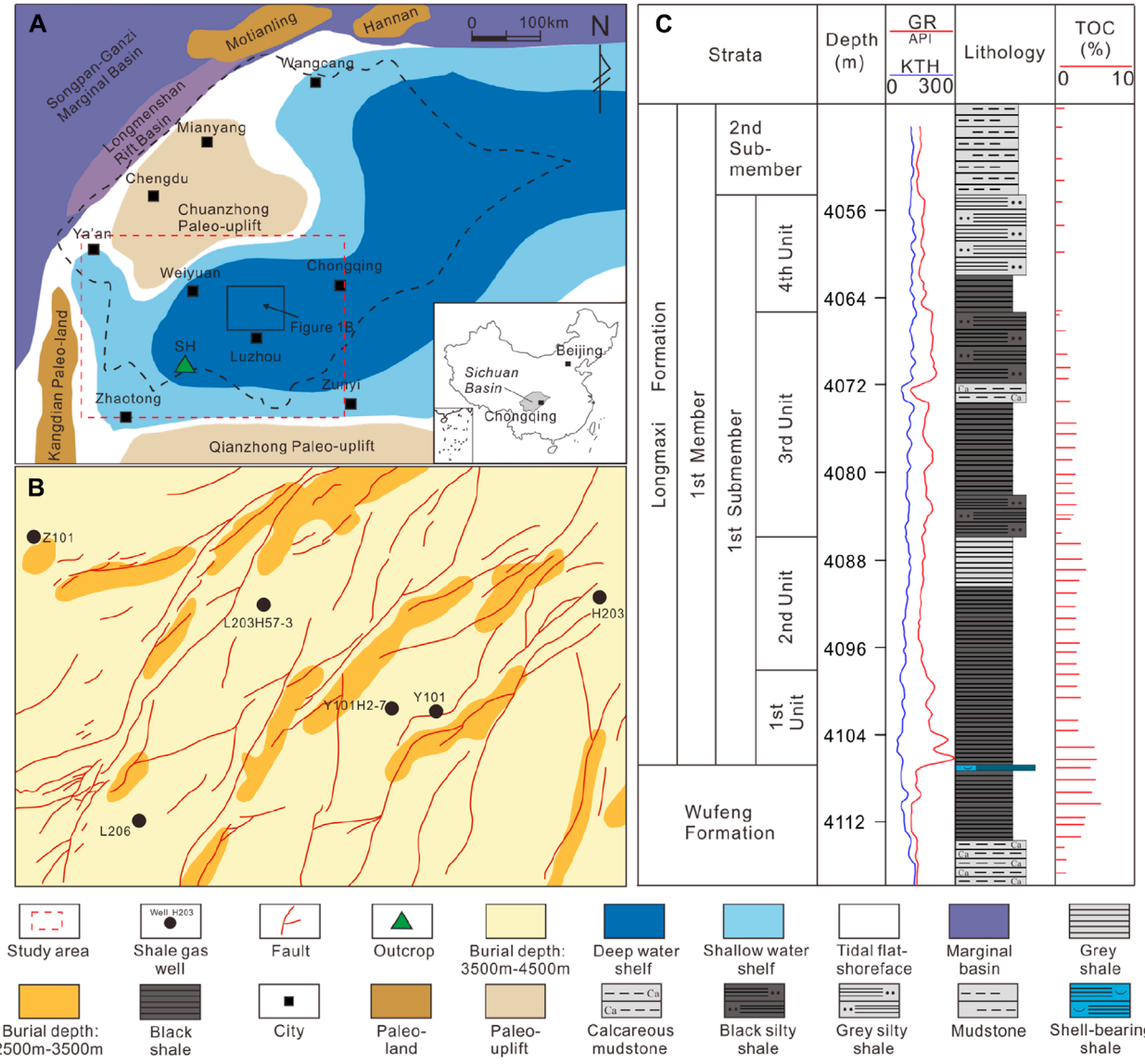

FIGURE 1
(A) Paleogeography of Wufeng-Longmaxi Formation in Sichuan Basin. **(B)** Fault distribution and burial depth of Wufeng-Longmaxi Formation (modified from Zou et al., 2016a; Dong et al., 2022). **(C)** Stratigraphic column of Wufeng-Longmaxi Formation in South Sichuan Basin.

in the study area varies significantly among different well areas. Macroscopically, large-scale faults can control the preservation of shale gas (Ma et al., 2023). Microscopically, fractures are beneficial for improving the permeability of shale gas reservoirs and are one of the important factors for shale gas wells to obtain commercial natural gas flow (Gao et al., 2020; Dong et al., 2022). According to sedimentary cycle, Longmaxi Formation can be divided into 1st Member and 2nd Member from bottom to top. The 1st Member is a progradational reverse cycle of continuous regression, and can be divided into two submembers based on lithologic characteristics and sedimentary cycle. To meet the needs of fine development, the 1st Submember is divided into four units: 1st Unit, 2nd Unit, 3rd Unit and 4th Unit based on petrological characteristics and logging characteristics (Figure 1C).

Samples and methods

Based on core observation and outcrop observation, four shale samples of Wufeng-Longmaxi Formation shale samples obtained from coring wells and outcrop. These samples were processed into 25 mm × 25 mm core-plug sample for nuclear magnetic resonance (NMR) experiment. The remaining samples are for field emission-scanning electron microscope (FE-SEM) identification, X-ray diffraction, low-temperature N_2 (LTNA) and CO_2 adsorption (LTCA) experiments and TOC measurement.

FE-SEM identification was carried out through a FEI Quanta 650 FEG type field emission scanning electron microscope produced in the United States. The whole-rock mineral X-ray diffraction measurement was carried out using a German Bruker D8 Advance

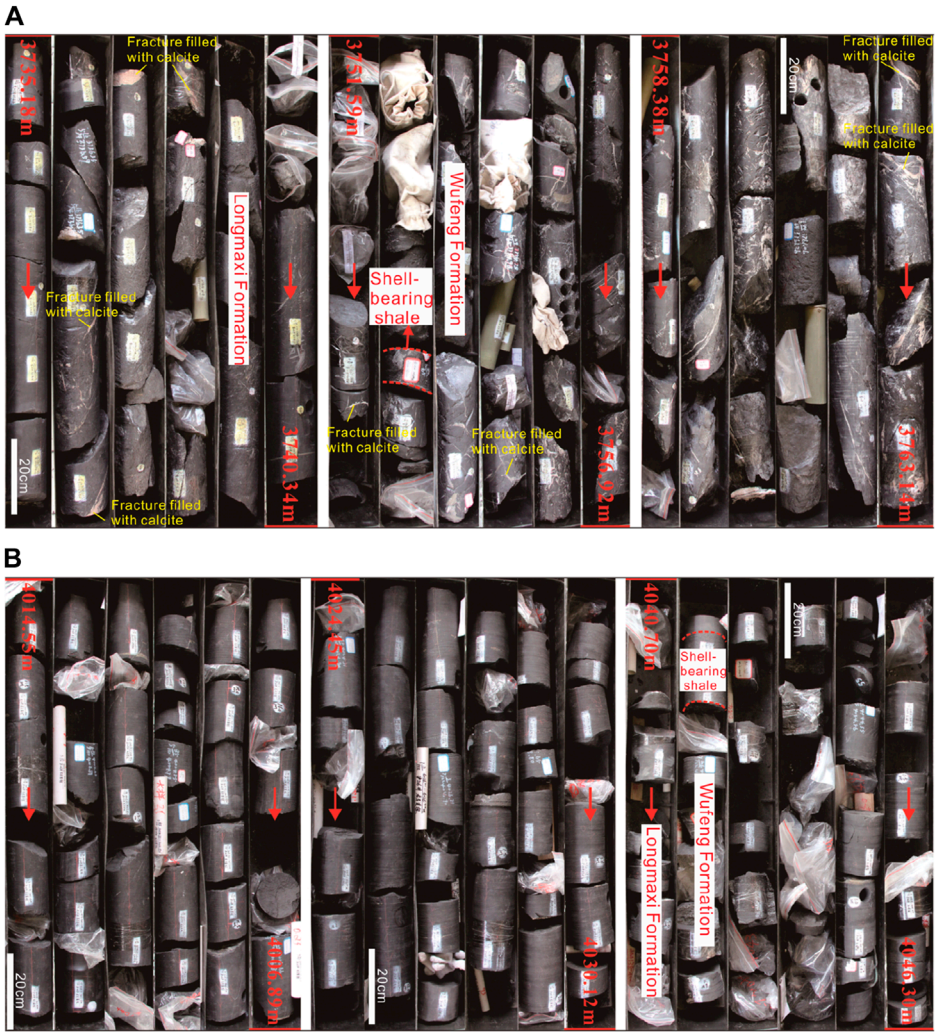

FIGURE 2
Macroscopic characteristics of marine shale interval in Wufeng-Longmaxi Formation. **(A)** The maximum fracture width can reach 6 mm, and the minimum is also 1 mm, 3,735.18 m–3763.14 m, Well H203. **(B)** The degree of fracture development is significantly low, 4,014.55 m–4046.30 m, Well L206.

X-ray diffractometer. TOC measurement was carried out through a LECO CS230 Series Carbon and Sulfur Analyzer. 4 core-plug samples of different shale lithofacies were implemented with NMR analysis in both dry and saturated brine states (including n-dodecane and brine) using a MacroMR12-150H-I low-field NMR device manufactured by the Suzhou Newmai Company. Low-temperature N_2 (LTNA) and CO_2 adsorption (LTCA) analyses are capable of characterizing nanoscale pores in porous media, and adsorption tests were performed with dried samples (60–80 mesh) on an Autosorb-IQ3 specific surface area (SSA) and pore size distribution (PSD) analyzer manufactured by the Cantor Company of the United States at Southwest Petroleum University. After the experiment, the Density functional theory (DFT) model was employed to obtain the pore size distribution and volume. The pore size was divided into three categories according to the pore size classification scheme (Loucks et al., 2012), namely micropores (<2 nm), mesopores (2 nm–50 nm), and macropores (>50 nm).

Influence of structural feature and fracture system on pore structure

Structural feature and fault system

So far, the Wufeng-Longmaxi marine shale has undergone multiple tectonic movements (Zhu et al., 2019; Fan et al., 2024). The Southern Sichuan Basin spans three secondary structural zones in terms of structure, with complex and variable structural characteristics that affect the development of shale reservoirs and the preservation of shale gas (Guo et al., 2021; Ma et al., 2023). The gas content and fracturing effect of shale reservoirs in different

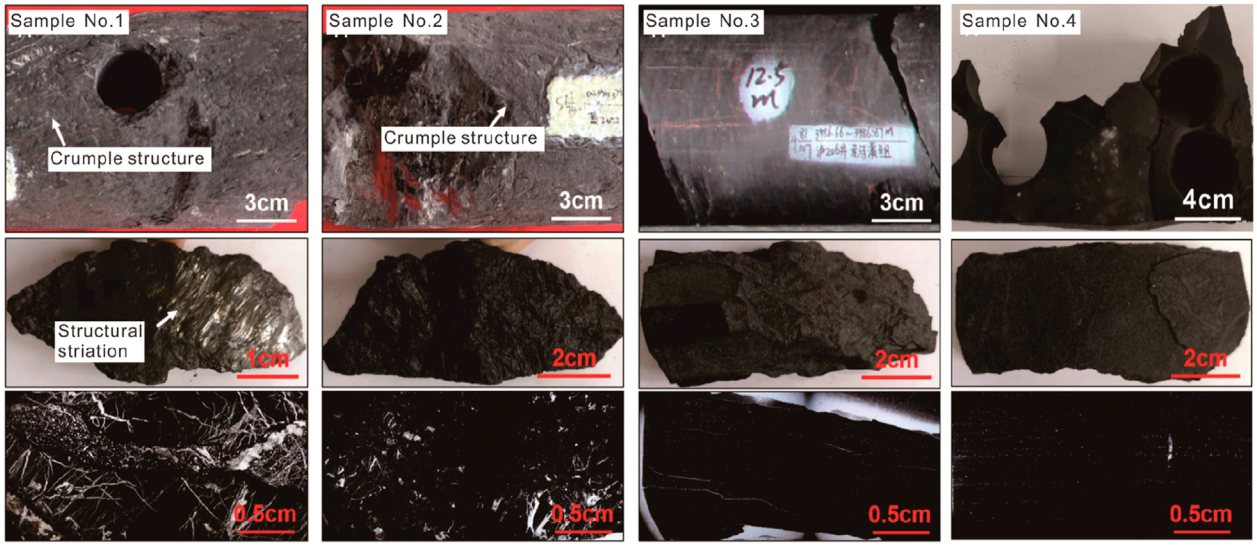

FIGURE 3
Petrological characteristics of marine shale interval in Wufeng-Longmaxi Formation.

TABLE 1 Basic parameters of the marine shale samples under different structural conditions.

Sample no.	Well/Outcrop	Depth (m)	Strata	TOC (%)	Mineral composition (%)			
					Quartz + Feldspar	Carbonate	Clay	Pyrite
1	H203	3,739.47	4th Unit	1.10	42.91	8.51	47.53	1.05
2	H203	3,740.87	4th Unit	1.17	43.14	7.88	47.97	1.01
3	L206	3,985.66	4th Unit	1.15	41.84	6.65	50.14	1.37
4	SH	—	4th Unit	1.21	43.10	6.12	49.15	1.63

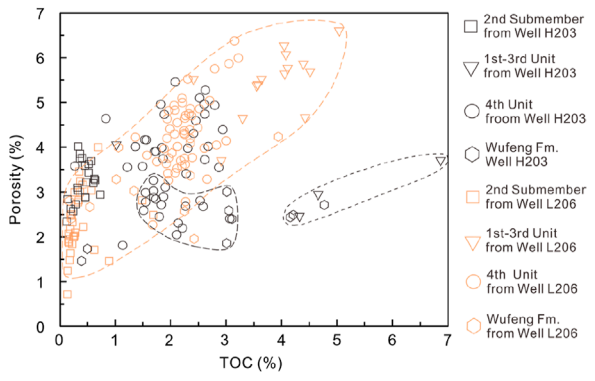

FIGURE 4
Comparison of shale porosity between the Wufeng-Longmaxi Formation of Well H 203 and Well L 206.

structural zones vary greatly, which also leads to significant differences in shale gas single well production capacity (Hu et al., 2017). To further study the influence and control of structural feature and fault system development on the pore structure of shale reservoirs, it is necessary to compare and analyze the similarities and differences in the pore structure characteristics of shale reservoirs under different structural conditions (Li, 2023a; Li, 2023b). A series of relatively tight anticlines in a northeast southwest direction and a series of wide and gentle synclines in the same direction are developed in the study area, with typical features of compound folds overall (Gao et al., 2020).

Well H203 is situated in the anticline's core extension, flanked by multiple northeast southwest trending fault zones. The drilling core indicates the presence of intense tectonic compression on the shale. Multiple stages of fractures are developed from the top of the Wufeng Formation to the top of the Longmaxi Formation. These fractures are mostly filled with calcite, and the local rocks are severely fractured, exhibiting typical features of mylonitic texture (Figure 2A). Shale gas production capacity is often closely related to the development of fractures (Fan et al., 2024). Shale intervals that have well-developed fractures, particularly those that naturally possess or can be induced to form fractures through hydraulic fracturing, are considered highquality reservoirs for shale gas (Wang et al., 2020; Zhou et al., 2022).

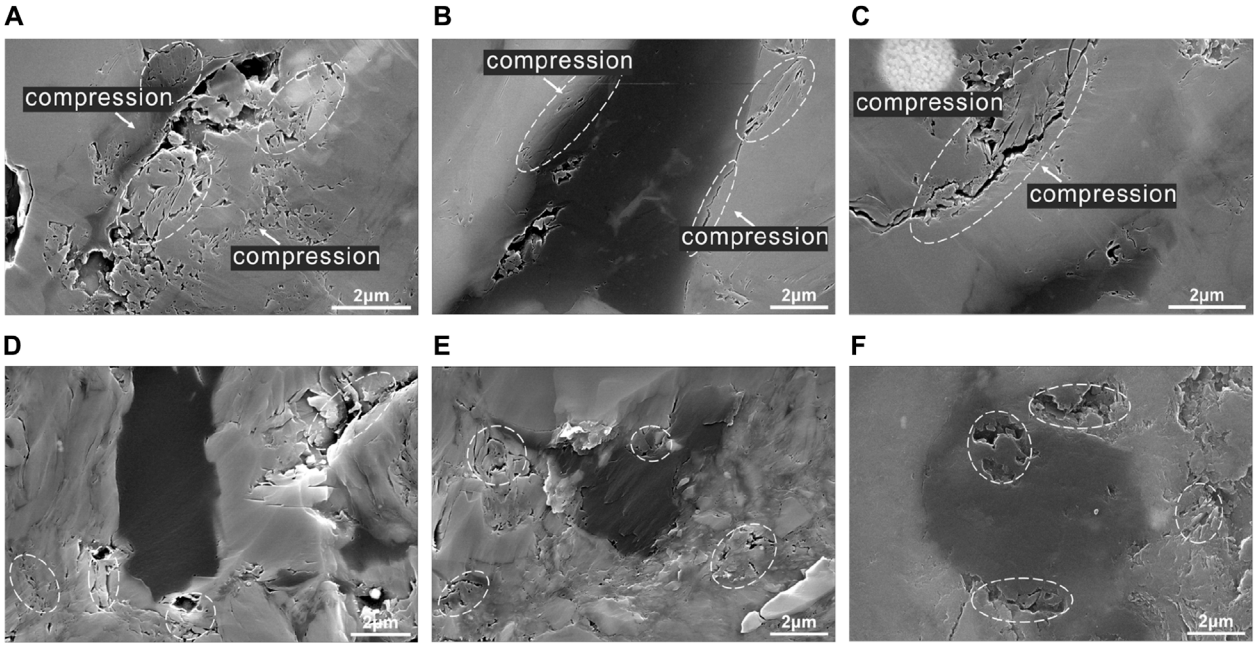

FIGURE 5
FE-SEM images of nanoscale pores and fractures in Wufeng-Longmaxi Formation shale. **(A)** Inorganic pores have directionality, Well H203, 3,740.86 m, 4th Unit. **(B)** The pores at the edge of organic matter have directionality, Well H203, 3,740.86 m, 4th Unit. **(C)** Fractures and oriented inorganic pores generated by compression, Well H203, 3,740.86 m, 4th Unit. **(D)** A large number of inorganic pores with no directional distribution, Well L206, 3,985.66 m, 4th Unit. **(E)** Non directional distribution of inorganic pores, Well L206, 3,985.66 m, 4th Unit. **(F)** Random distribution of pores, no compression characteristics, and underdevelopment of organic pores, SH Outcrop.

Well L206, at the core of the syncline, is distant from the significant fault, ensuring stable structural circumstances. Drilling core observations confirm absence of substantial fractures or notable structural compression features in the Wufeng-Longmaxi Formation (Figure 2B). A limited number of tensile fractures emerge in specific depth intervals, maintaining a well-preserved shale with distinct bedding plane (Figure 3).

Samples No. 1 and No. 2 were selected from the 4th Unit of Longmaxi Formation in Well H203. Severe structural compression resulted in severe fragmentation of the 4th Unit rock core, with developed structural wrinkling. Smooth structural compression scratches can be seen along the bedding, and a large number of cracks filled with calcite can be seen at the microscopic scale. Sample No. 3 was collected from the 4th Unit of Well L206, which is far from the fault. There is no significant structural compression or fracture development on the rock core, which belongs to the normal sample. Sample No. 4 was collected from Outcrop SH, and no fractures caused by compression characteristics were observed (Figure 3). The basic parameters of the four samples are shown in Table 1, and the TOC content is relatively low and close, with values of 1.10%, 1.17%, 1.15%, and 1.21%, respectively. The mineral composition is not significantly different, mainly composed of clay and siliceous minerals (quartz + feldspar), with contents ranging from 47.53% to 50.14% and 41.84%–43.14%, respectively. The content of carbonate rocks and pyrite is relatively low, with distribution ranges of 6.12%–8.51% and 1.05%–1.63%, respectively.

Effect on pore structure

The cross-plot of TOC content vs. porosity suggest that the shale porosity of Well L206 shows an increasing trend with the increase of TOC (Figure 4). 1st, 2nd and 3rd Unit has the highest TOC content and highest porosity. By comparison, the porosity range of Well H203 is between 1.5% and 5.0%, and does not show an increasing trend with the increase of TOC. The porosity of some samples from the Wufeng Formation and the 4th Unit showed a decreasing trend, significantly lower than that of shale samples with similar TOC content in Well L206. These shale samples are precisely distributed in the intervals with intense tectonic compression. Therefore, from the perspective of porosity, it is suggested that strong tectonic compression can reduce the size of porosity, leading to poorer pore development.

Shale samples were selected from Well H203, Well L206, and Outcrop SH for comparative analysis to further discuss the effect of tectonic action on pore structure. Firstly, after polishing and gold plating the samples, characteristics of pores and microfractures were observed by FE-SEM. The results indicate that the No. 1 and No. 2 samples, which were strongly compressed by the structure, developed directional narrow slit-shaped pores, with the long axis of the pores pointing in the same direction. Meanwhile, rigid mineral particles are crushed by compression and microfractures are formed by tectonic action (Figures 5A–F). The other samples also develop a large number of nano-scale and micro-scale mineral

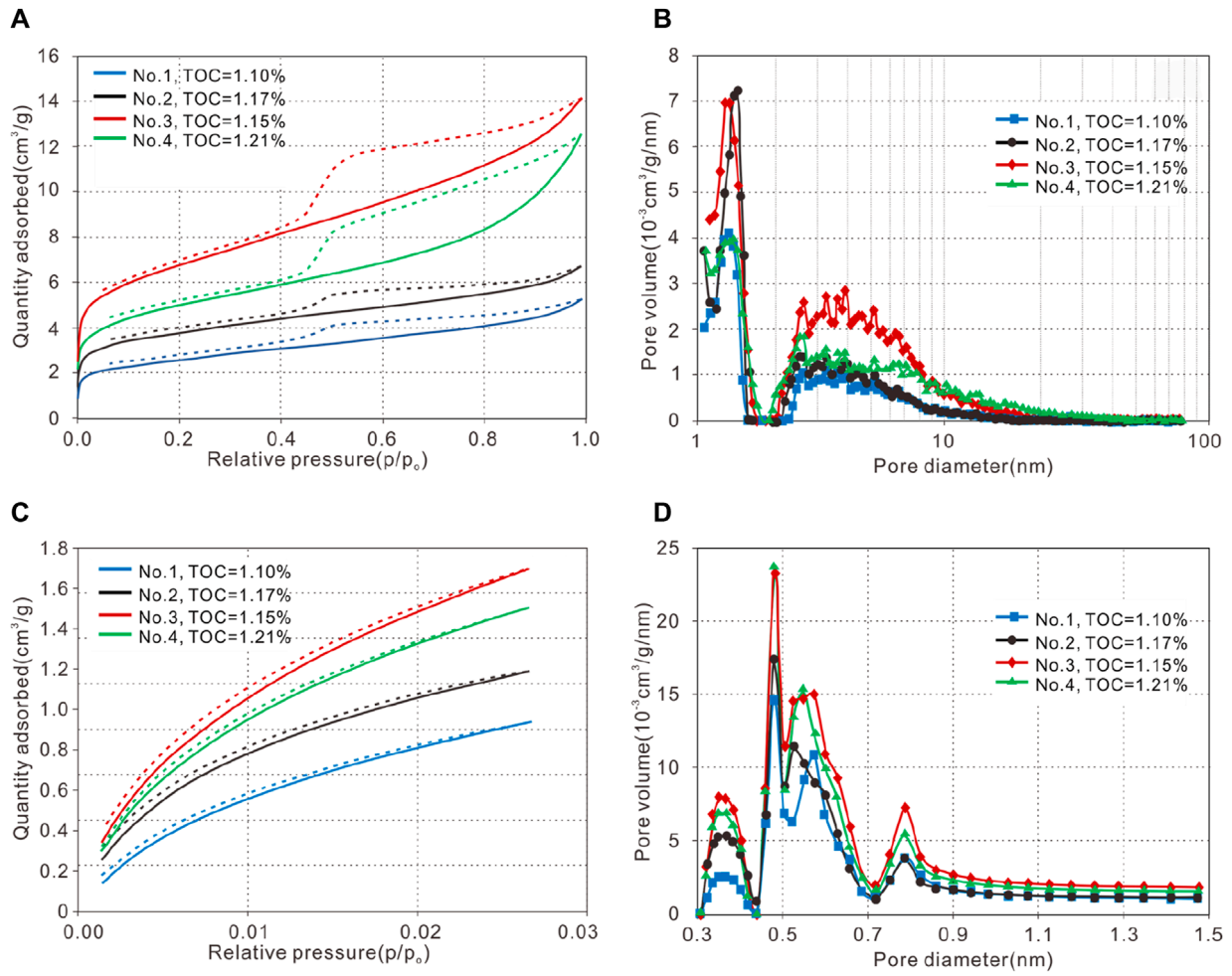

FIGURE 6
Pore structure characteristics of Wufeng-Longmaxi Formation shale by LTNA and LTCA. **(A)** LTNA curves. **(B)** Pore size distribution curve by LTNA. **(C)** LTCA curve. **(D)** Pore size distribution curve by LTCA.

related pores. But these pore distributions have no directionality, and the pore morphology shows no narrow slit-like characteristics, and microfractures are relatively rare (Figures 5A–F).

LTNA and LTCA adsorption experiments were conducted on four samples, and corresponding adsorption desorption curves and pore size distribution curves were obtained. The adsorption and desorption processes shown by the N_2 adsorption curve are influenced by the size and morphology of the nanopores, so the hysteresis loop generated during the N_2 adsorption-desorption process can reflect the morphology of the pores (Sing et al., 1985). The IUPAC classification of LTNA curves and hysteresis loops divides nanoscale pores into four different categories, i.e., cylindrical pores, ink bottle pores, parallel plate pores, and slit pores (Thommes et al., 2015). The hysteresis loops of No. 1 and No. 2, which are affected by strong structural compression, are flatter and belong to the typical H_3-H_4 type according to IUPAC classification, corresponding to parallel plate pores and slit pores between rigid aggregates composed of sheet-like particles. In contrast, No. 3 and No. 4 is characterized by plump hysteresis loops, reflecting cylindrical pores and ink bottle pores. This result is consistent with the observation of FE-SEM (Figure 6A). The pore volume increment data of micropores, mesopores, and macropores with pore sizes between 1 nm and 100 nm were obtained based on the NLDFT model. In the pore size range greater than 3 nm, the pore volume increment of No. 1 and No. 2 is significantly lower than that of No. 3 and No. 4, while this phenomenon is not observed below 3 nm (Figure 6B).

With the continuous increase of relative pressure, the CO_2 adsorption capacity continues to increase, but the rate of increase in adsorption capacity gradually decreases. The isothermal adsorption trend between different samples is consistent, and according to previous classification schemes, the isothermal adsorption curve belongs to a typical Type I, indicating the development of micropores in shale samples. The isothermal CO_2 adsorption capacity of No. 1 and No. 2 is significantly lower than that of No. 3 and No. 4 (Figure 6C). The DFT model was used to obtain the distribution of pore volume increment in the range of 0.30 nm–1.50 nm. Comparing the pore volume ranges of the four

TABLE 2 Pore structure parameters obtained by different experimental methods.

Sample no.	LTCA		LTNA		SSA (m^2/g)	PV (10^{-3} cm^3/g)	NMR		
	SSA_{BET} (m^2/g)	PV_{DFT} (10^{-3} cm^3/g)	SSA_{BET} (m^2/g)	PV_{NLDFT} (10^{-3} cm^3/g)			Peak shape	Left peak area proportion (%)	Right peak area proportion (%)
1	5.11	3.13	9.14	4.45	14.25	7.58	Bimodal	88.33	11.67
2	5.84	3.69	13.49	5.18	19.33	8.87	Bimodal	89.06	10.94
3	7.96	5.46	24.06	12.52	32.02	17.98	Bimodal	83.24	16.76
4	7.32	4.79	17.87	13.28	25.19	18.07	Bimodal	84.14	15.86

samples, it is suggested that the pore volume increment of No. 3 and No. 4, which are not significantly compressed, is higher than that of No. 1 and No. 2 (Figure 6D).

According to the statistical results of specific surface area (SSA) and pore volume (PV), the SSA of No. 1 and No. 2 are 14.25 m^2/g and 19.33 m^2/g, respectively, and the PV is 7.58 × 10^{-3} cm^3/g and 8.87 × 10^{-3} cm^3/g. The SSA of No. 3 and No. 4 are 32.02 m^2/g and 25.19 m^2/g, respectively, and the PV is 17.08 × 10^{-3} cm^3/g and 18.07 × 10^{-3} cm^3/g (Table 2). The PV and SSA of samples No. 1 and No. 2 are significantly lower than those of samples No. 3 and No. 4.

Due to its limitation in detecting pores below 100 nm, isothermal adsorption is inadequate for evaluating pores exceeding this diameter. Therefore, based on isothermal adsorption, NMR was used to characterize the pore structure. Firstly, four shale samples were evacuated using a molecular pump. Then, the shale samples were saturated with low salinity brine under high pressure conditions. Finally, the NMR T_2 spectra in the saturated state were measured. The relaxation time of T_2 spectrum corresponds to the pore size distribution. At the same relaxation time, a higher signal amplitude indicates more pores with the same pore size, and a larger total pore volume (Zheng et al., 2020; Zhang et al., 2021). The T_2 spectra of the four samples exhibit a "bimodal" characteristic, with the left peak being the main peak corresponding to relatively small pores. The left peak is characterized by high signal amplitude and the largest area. The right peak is a secondary peak, with a lower peak height and smaller area for relatively large pores and microfractures (Figure 7). After calculating the area proportions of the left and right peaks, it can be found that the left peak proportions of No. 1 and No. 2 are higher than those of No. 3 and No. 4, and the right peak proportions are relatively lower (Table 2). Therefore, shale samples that have not been compressed have more "relatively large pores," or in other words, a larger proportion of "relatively large pores." After structural compression, some of the "relatively large pores" in the shale are converted into "relatively small pores," resulting in an increase in the proportion of "relatively small pores."

In general, strong structural compression is not conducive to the development and preservation of pores. Structural compression is an important factor leading to a decrease in pore size and volume, manifested in a decrease in porosity. In areas far away from structural compression and fault zones, shale preservation conditions are better, with more and larger pores and higher porosity, which is conducive to shale gas enrichment.

Effect of burial depth

Burial depth characteristics

Marine shale in this study area spans multiple depths, significantly differing in depth of burial. Due to the significant impact of geological compaction on reservoir space (Chen et al., 2022), exploring the pore structure characteristics under different burial depths is of great significance. This study evaluated the influence of burial depth on pore structure via comparative analysis of porosity, PV, and SSA due to massive organic/inorganic pore development in varying depths (Figure 8). The coupling relationship between porosity and burial depth was discussed based on the burial depth, TOC (Figure 8A), and porosity of shale samples from different areas. In different TOC intervals (Figure 8B), as the burial depth gradually increases from 1,000 m to 3,500 m, and then to 4500 m (Figure 8C), the overall porosity shows a decreasing trend, but the decrease is relatively limited. Shale porosity above 3,500 m is mostly distributed between 1% to 6%, slightly lower than 3%–7% below 3,500 m (Figure 8D). Moreover, certain samples buried at depths of 3,500 m–4,000 m retain high porosity, exceeding that of shale below 3,500 m (Table 3).

Effect on pore structure

In order to eliminate the influence of TOC and highlight the effect of burial depth on pore structure parameters represented by PV, SSD, and PSD, the PV, SSA and other parameters are normalized using TOC values. As the burial depth increases, the TOC normalized-SSA_{BET} overall shows a decreasing trend, especially for

TABLE 3 Burial depth and pressure coefficient of Wufeng-Longmaxi Formation in Sichuan Basin and surrounding areas.

Area	Burial depth (m)	TOC (%)	Porosity (%)	Pressure coefficient	References
Changning	2,510	4.15	7.09	2.03	this study
	2,385	4.04	5.19	1.35	
	1,311	3.45	5.22	0.96	
	3,115	4.23	5.32	1.29	
	2,225	4.08	5.32	1	
	2,327	4.82	6.44	1.3	
	3,115	3.73	5.04	1.51	
	2,746	3.6	5.14	1.8	
	2,353	3.59	4.08	1.12	
	3,046	3.21	4.11	1.74	
	3,414	3.82	5.51	2.08	
Luzhou	3,450	3.46	4.43	1.94	this study
	3,330	3.46	5.8	2.08	
	3,680	3.18	3.35	2.14	
	4,016	2.92	4.07	2.08	
	4,308	—	6	2.24	Yang et al. (2019)
	3,530	3.4	4.33	2.25	
	3,851	3.44	4.61	2.1	
	3,480	3.45	4.65	2.19	
Southeast Sichuan Basin	2,160	3.31	2.91	0.96	Wu et al. (2022)
	2,415	3.93	4.69	1.46	
	4,411	3.17	4.12	1.35	
	2,575	3.71	6.2	1.55	
	2,596	3.65	6.19	1.55	
	2054	3.42	3.03	1.06	
	4,368	3.95	5.94	1.55	
	780	3.02	3.27	0.57	
	580	2.05	3.57	1.12	
	2,208	2.54	2.8	1.1	
	2,750	3.4	2.95	1	

(Continued on the following page)

TABLE 3 (*Continued*) Burial depth and pressure coefficient of Wufeng-Longmaxi Formation in Sichuan Basin and surrounding areas.

Area	Burial depth (m)	TOC (%)	Porosity (%)	Pressure coefficient	References
Weiyuan	1,523	2.61	3.65	0.92	Zhang (2019)
	3,015	4.11	4.26	1.40	
	3,171	3.37	4.19	1.77	
	3,776	3.31	5.28	1.96	
	3,470	2.92	4.15	2.2	
Zhaotong	2055	3.32	3.94	0.98	Zhang (2019)
	1,231	2.70	4.21	1.15	

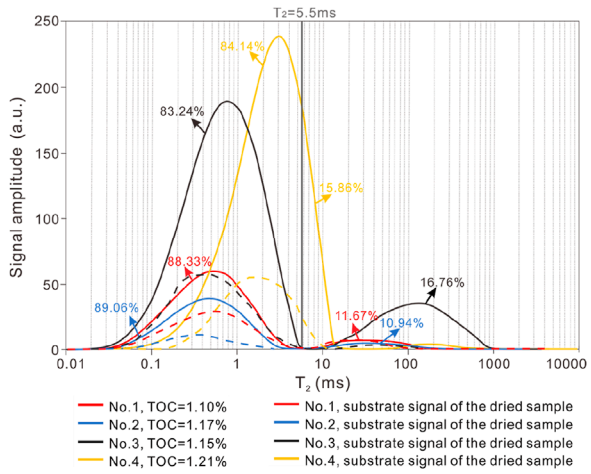

FIGURE 7
NMR T_2 spectra of shale samples saturated with low salinity brine.

samples with high TOC (3%–6%), where the decreasing trend is more evident. Meanwhile, there are also outliers, such as several outcrop samples with shallow burial depths (close to 0 m), but their normalized-SSA_{BET} is not higher than that of samples with depths greater than 3500 m, and the distribution of data points is relatively scattered (Figure 9). This may be attributed to the weathering effect on the outcrop samples.

The TOC normalized-PV_{BJH} is more strongly influenced by burial depth. As the burial depth increases, the trend of decreasing normalized-PV_{BJH} becomes more significant. Under conditions greater than 3500 m, the distribution of normalized-PV_{BJH} tends to be concentrated (Figure 9A), which is similar to the statistical results of porosity. The normalized-PV_{BJH} of high TOC samples is relatively lower (Figure 9B). For example, in samples with TOC ranging from 3% to 6%, the normalized-PV_{BJH} is distributed between 2 × 10^{-3} cm^3/g and 4 × 10^{-3} cm^3/g (Figures 9C, D), which is lower than in samples with TOC ranging from 1% to 3% (3 × 10^{-3} cm^3/g to 8 × 10^{-3} cm^3/g) (Figures 9A, B), reflecting a large number of inorganic pores in shale. As the organic matter content increases, the proportion of PV in inorganic pores decreases relatively. After normalization, the total PV of shale with high organic matter content is closer to the PV of organic pores (Figure 10). The increase in burial depth will amplify the compaction effect and inevitably enhance the destructive effect on pores. Despite factors such as high brittle mineral content and formation over-pressure that resist compaction, excessive burial depth is still a controlling factor for poor pore development.

Formation pressure coefficient

The planar distribution map of burial depth and pressure coefficient of marine shale in the study area shows that there are significant differences in burial depth and pressure coefficient among different regions. In areas close to faults and erosion zones, the burial depth of shale is small. Shale gas inevitably experiences leakage and dissipation, leading to generally low pressure coefficients, such as Well N208 and N210 in Changning area. According to the pressure coefficient classification scheme (Fu, 2016; Chen et al., 2020; Jin et al., 2023), it can be divided into five intervals from low to high: low pressure, atmospheric pressure, slight over-pressure, over-pressure, and strong over-pressure, with distribution ranges of <0.8, 0.80–1.2, 1.2–1.5, 1.50–1.73, and >1.73, respectively (Table 4).

Most areas in the Southern Sichuan Basin falls within the four ranges of atmospheric pressure, slight over-pressure, over-pressure, and strong over-pressure. Due to differences in conditions such as erosion zones, faults, and burial depths, the pressure coefficient varies significantly. The Zhaotong area, located outside the basin, has a large number of erosion zones with the lowest burial depth and pressure coefficient, belonging to atmospheric pressure and slight over-pressure. The part near the erosion zone in Changning area is under atmospheric pressure, and the pressure coefficient of the Southern Changning area centered around Well N201 is high, belonging to over-pressure and strong over-pressure. The shale in Luzhou area has a large burial depth and high pressure coefficient, belonging to strong over-pressure, with an

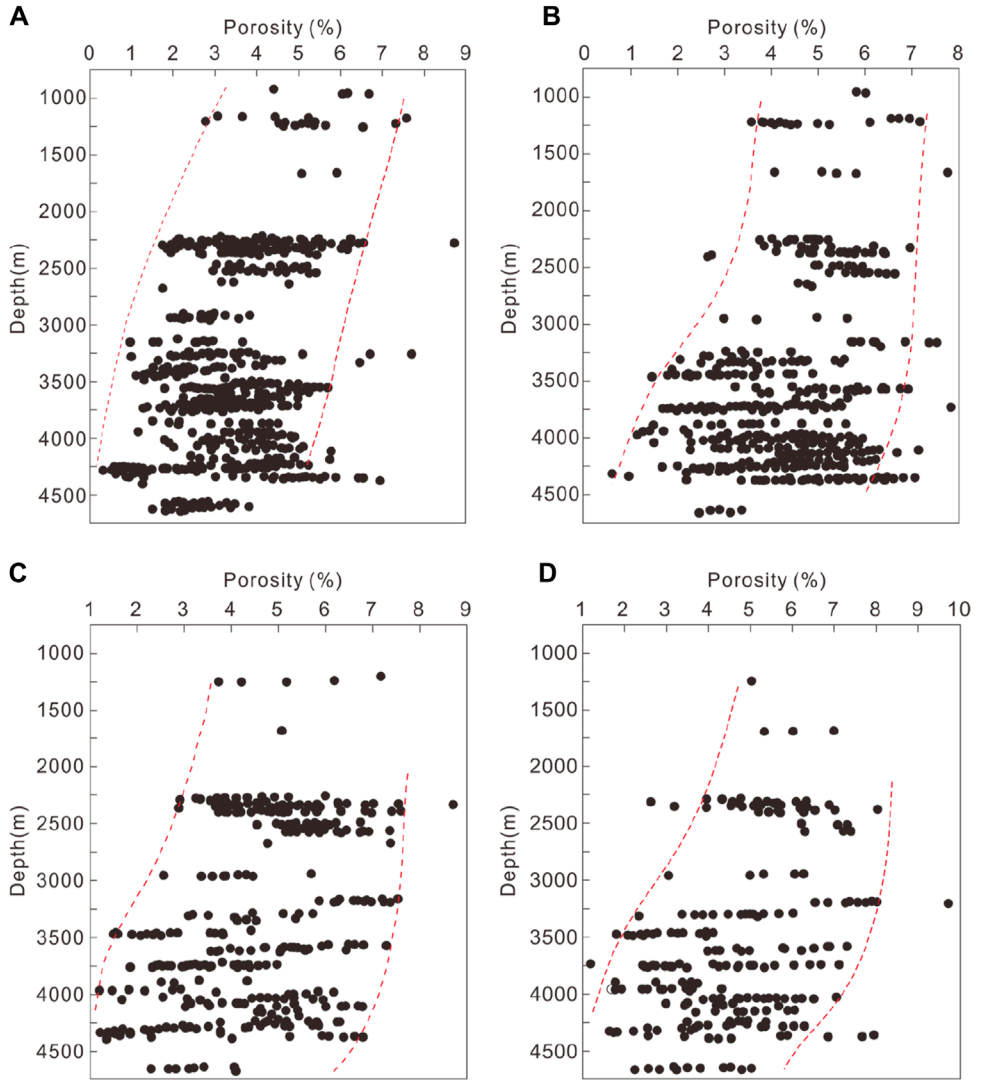

FIGURE 8
The relationship between shale porosity and burial depth in the Wufeng-Longmaxi Formation. **(A)** TOC value between 1% -2%; **(B)** TOC value between 2% -3%; **(C)** TOC value between 3% -4%; **(D)** TOC value between 4% -6%.

average pressure coefficient of over 1.80. The Weiyuan area in the northernmost part of the study area, due to its proximity to the pinch-out line and shallow burial depth (such as the Well W201), has a low pressure coefficient, and is mainly characterized by atmospheric to slight over-pressure along the pinch-out line. The Southern Weiyuan area is adjacent to Luzhou area, and the closer it is to Luzhou area, the deeper it is buried. In addition, the fault system and erosion zone in the Southern Weiyuan area are underdeveloped, and the pressure coefficient is generally high (>1.50), belonging to strong over-pressure (Figure 11).

As shown in Figure 12, the relationship between the burial depth and pressure coefficient of the Wufeng-Longmaxi Formation shale indicates that as the burial depth increases, the pressure coefficient shows an increasing trend. There is a positive correlation between the two (R^2 = 0.5281). For example, the Luzhou area has the highest burial depth and pressure coefficient. However, there are also cases where the burial depth is large but the formation pressure coefficient is relatively low, and these wells are mainly distributed in the southeastern part of the Sichuan Basin. It is speculated that the complex structural characteristics of these regions are related to the rich fault system leading to shale gas leakage, resulting in abnormally low pressure coefficients (Tang et al., 2015).

Discussion

As mentioned above, excessive burial depth of shale is an important factor in damaging the porosity and pore structure parameters of shale reservoirs. Considering the correlation between

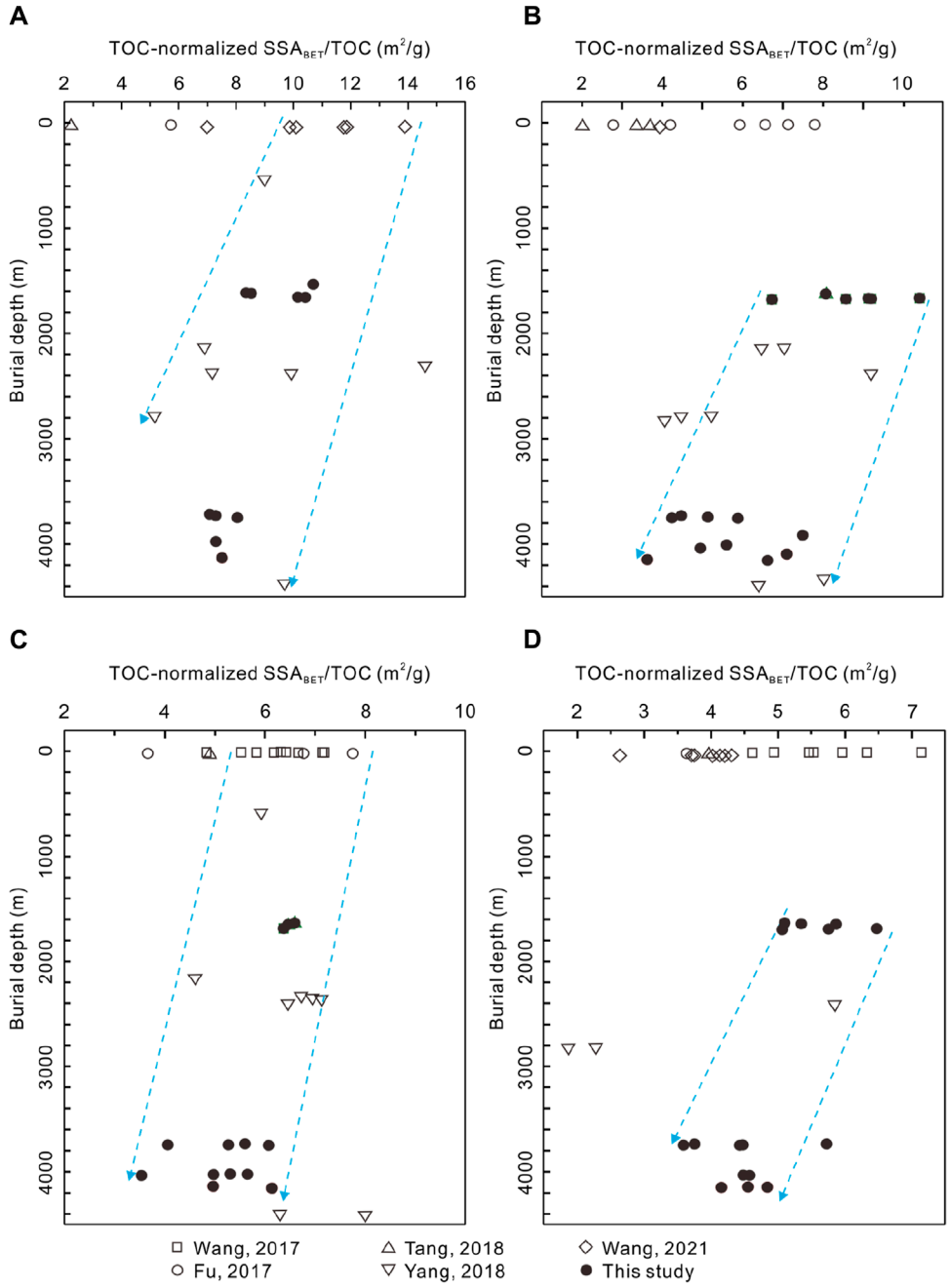

FIGURE 9
The relationship between the specific surface area (SSA) and burial depth of shale in the Wufeng-Longmaxi Formation (Most of the data is cited from Fu, 2017; Tang, 2018; Wang, 2017; Wang, 2021; Yang, 2018). **(A)** TOC=1%–2%. **(B)** TOC=2%–3%. **(C)** TOC=3%–4%. **(D)** TOC=4%–6%.

burial depth and pressure coefficient (Qiu et al., 2020), it is necessary to discuss the relationship between pressure coefficient and shale reservoir parameters. From the perspective of porosity, as the burial depth increases, the pressure coefficient shows an increasing trend, which is consistent with the statistical results mentioned earlier. In this study, the burial depth was divided into three intervals:<3,000 m, 3,000 m–3500 m, and >3500 m, respectively, to discuss the relationship between porosity and formation pressure coefficient. When the burial depth of shale is less than 3,000 m, the porosity shows an increasing trend with the increase of burial depth and pressure coefficient. However, when the shale burial depth further increases to over 3,000 m, the overall formation pressure coefficient has reached 1.4 or above. At this time, the distribution of shale porosity is relatively concentrated, ranging from 2% to 6%, with vast majority of porosity distributed between 2% and 5%. There was no trend of porosity increasing with the

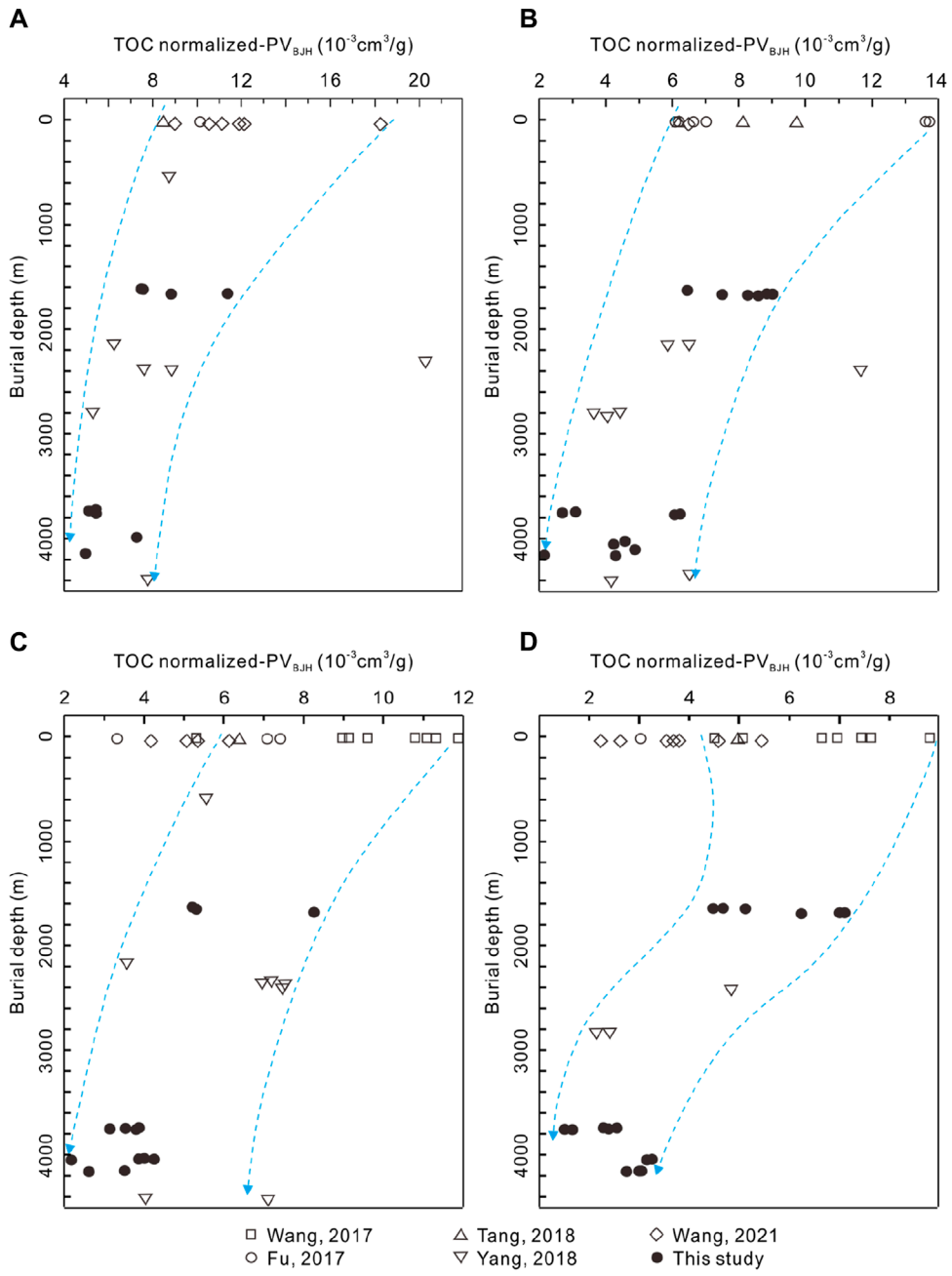

FIGURE 10
The relationship between the pore volume (PV) and burial depth of shale in the Wufeng-Longmaxi Formation (Most of the data is cited from Fu, 2017; Tang, 2018; Wang, 2017; Wang, 2021; Yang, 2018). **(A)** TOC=1%-2%. **(B)** TOC=2%-3%. **(C)** TOC=3%-4%. **(D)** TOC=4%–6%.

increase of pressure coefficient. Further analysis suggests that as the burial depth increases, the compaction effect of the overlying strata will increase, and the formation pressure coefficient will also increase. The pressure coefficient/formation over-pressure and formation compaction show a mutually weakening effect. However, when the burial depth reaches a certain threshold (>3000 m), the compaction effect of the overlying strata and the damage preservation effect of over-pressure on pores reach a balance. The protective effect of over-pressure on pores is relatively limited, and the distribution of porosity shows a relatively concentrated feature (Figure 13). Based on the influence of burial depth on pore structure parameters, especially PV, it is speculated that this phenomenon is also applicable to shale pore structure.

TABLE 4 Classification scheme for formation pressure coefficient (Fu, 2016; Chen et al., 2020; Jin et al., 2023).

Classification	Level	Pressure gradient (kPa)	Pressure coefficient
I	Low pressure	<10.00	<0.8
II	Atmospheric pressure	10.00–12.00	0.8–1.2
III	Slight overpressure	12.00–15.00	1.2–1.5
IV	Overpressure	15.00–17.30	1.50–1.73
V	Strong overpressure	>17.30	>1.73

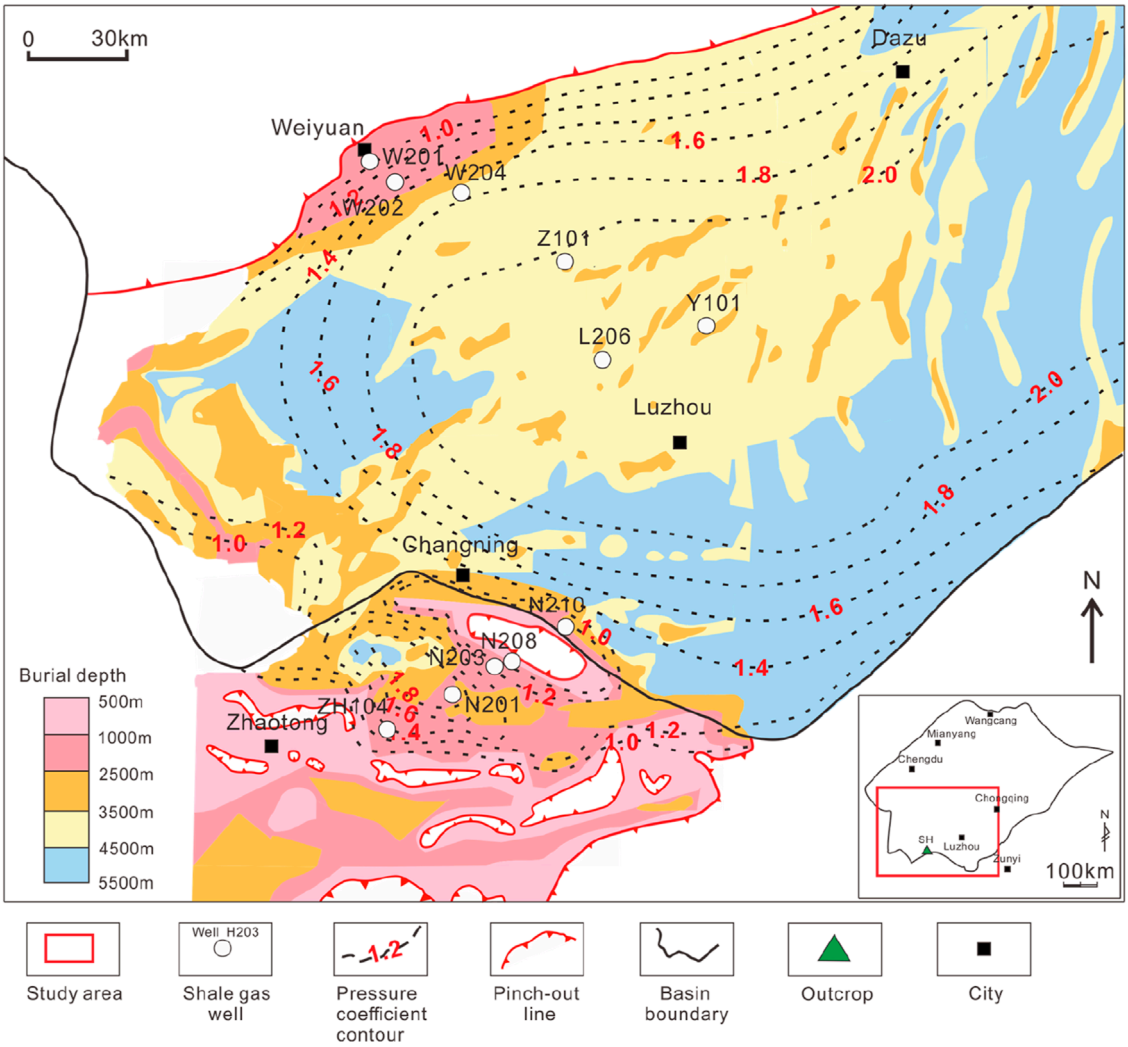

FIGURE 11
Distribution characteristics of burial depth and pressure coefficient of shale formations in the Wufeng-Longmaxi Formation of the study area (modified from Zou et al., 2016a; Zou et al., 2016b; Tang et al., 2022).

Conclusion

1) Stable structural conditions facilitate pore development and preservation in shale reservoir. Under the influence of structural compression, deformation within the shale occurs, reducing inorganic and organic pores into narrowed and elongated forms with directional pore distribution and intensified micro-fracture evolution. Shale samples

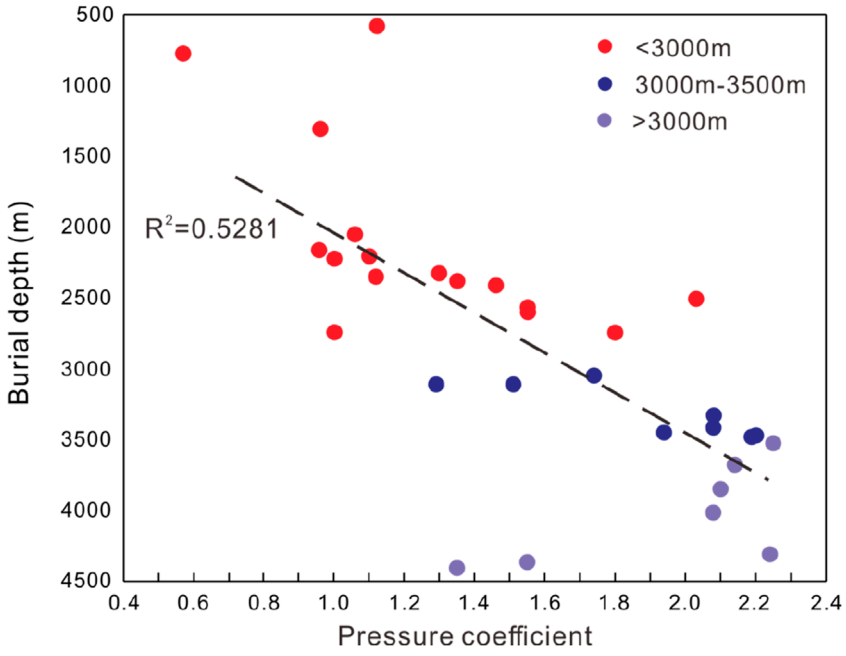

FIGURE 12
The relationship between the burial depth of the Wufeng-Longmaxi Formation and the formation pressure coefficient.

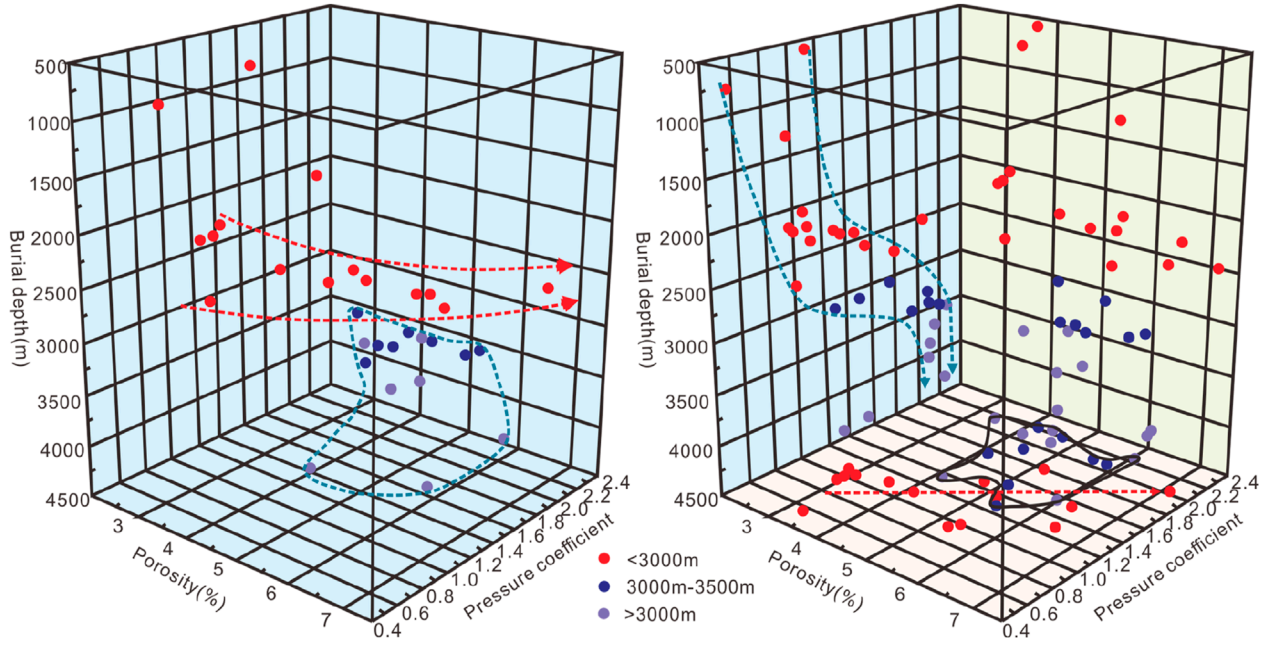

FIGURE 13
Coupling relationship between different burial depths, pressure coefficients, and shale porosity in the Wufeng-Longmaxi Formation.

with stable structural conditions displays elevated porosity compared to compressed shale samples. Under similar TOC content and mineral composition, the pore size distribution curve of shale under structural compression shows significantly lower micropores and mesopores than other samples. The pore volume and specific surface area of shale under tectonic compression rank lower compared to others. The peak area on the right side of the T_2 spectrum of saturated saline corresponds to the proportion of relative macropores and micro-fractures in the total pore volume. Shale samples subjected to structural compression exhibited significantly diminished pore volumes compared to other shale

counterparts, implying substantial shrinkage in the volume of expanded pores and micro-fractures.

2) As burial depth escalates, shale reservoir porosity exhibits a declining pattern, yet the reduction is restrained. Shale reservoir porosity with a burial depth of less than 3500 m ranges from 3% to 7%, while shale porosity with a burial depth of more than 3500 m ranges from 1% to 6%. Burial depth has a significant impact on the specific surface area and pore volume of high TOC shale (3%–6%). Burial depth causes a discernible decline in both specific surface area and pore volume. Upon reaching a shale burial depth of 4000 m, the distribution of pore volume and specific surface area data points becomes more concentrated. The pressure coefficient visualizes the shale pore development and preservation status. The higher the pressure coefficient, the better the preservation conditions of the shale reservoir, and the higher the shale porosity. The pressure coefficient is positively correlated with porosity. High pressure coefficient can slow down the compaction effect of overlying strata, and moderate burial conditions play an important role in protecting the pores.

Data availability statement

The raw data supporting the conclusion of this article will be made available by the authors, without undue reservation.

Author contributions

WY: Conceptualization, Investigation, Writing–original draft. SY: Methodology, Visualization, Writing–original draft. HT: Data curation, Investigation, Software, Writing–review and editing. CL: Formal Analysis, Methodology, Software, Writing–review and editing. WW: Project administration, Validation, Visualization, Writing–review and editing. JL: Conceptualization, Investigation, Methodology, Writing–original draft. YY: Data curation, Investigation, Software, Writing–review and editing. KZ: Conceptualization, Methodology, Visualization, Writing–original draft. LH: Data curation, Investigation, Methodology, Writing–review and editing.

Funding

The author(s) declare financial support was received for the research, authorship, and/or publication of this article. This study was funded by the Innovation Consortium Project of China National Petroleum Corporation and Southwest Petroleum University (Grant No. 2020CX020102).

Conflict of interest

Authors WY, SY, CL, WW, JL, YY, KZ, and LH were employed by PetroChina Southwest Oil and Gasfield Company.

The remaining author declares that the research was conducted in the absence of any commercial or financial relationships that could be construed as a potential conflict of interest.

The reviewer HL declared a shared affiliation with the author HT to the handling editor at the time of review.

Publisher's note

All claims expressed in this article are solely those of the authors and do not necessarily represent those of their affiliated organizations, or those of the publisher, the editors and the reviewers. Any product that may be evaluated in this article, or claim that may be made by its manufacturer, is not guaranteed or endorsed by the publisher.

References

Cai, G., Gu, Y., Jiang, Y., and Wang, Z. (2023). Pore structure and fluid evaluation of deep organic-rich marine shale: a case study from Wufeng-Longmaxi Formation of Southern Sichuan Basin. *Appl. Sci.* 13 (13), 7827. doi:10.3390/app13137827

Chalmers, G. R., Bustin, R. M., and Power, I. M. (2012). Characterization of gas shale pore systems by porosimetry, pycnometry, surface area, and field emission scanning electron microscopy/transmission electron microscopy image analyses: examples from the Barnett, Woodford, Haynesville, Marcellus, and Doig units. *AAPG Bull.* 96 (6), 1099–1119. doi:10.1306/10171111052

Chen, F., Duan, J., Zhang, H., Wei, X., Liu, Z., Wang, Q., et al. (2020). Shale gas resource evaluation based on "pressure coefficient": a case study of Upper Ordovician Wufeng-Lower Silurian Longmaxi formations in southeastern Sichuan Basin. *Pet. Geology&Experiment* 42 (3), 405–414. doi:10.11781/sysydz202003405

Chen, Y., Tang, H., Liao, J., Luo, C., Zhao, S., Zheng, M., et al. (2022). Analysis of shale pore characteristics and controlling factors based on variation of buried depth in the Longmaxi Formation, Southern Sichuan Basin. *Geol. China* 49 (2), 472–484. doi:10.12029/gc20220209

Dong, D., Liang, F., Guan, Q., Jiang, Y., Zhou, S., Yu, R., et al. (2022). Development model and identification evaluation technology of Wufeng-Longmaxi Formation quality shale gas reservoirs in the Sichuan Basin. *Nat. Gas. Ind.* 42 (8), 96–111. doi:10.3787/j.issn.1000-0976.2022.08.008

Fan, C. H., Nie, S., Li, H., Radwan, A. E., Pan, Q. C., Shi, X. C., et al. (2024). Quantitative prediction and spatial analysis of structural fractures in deep shale gas reservoirs within complex structural zones: a case study of the Longmaxi Formation in the Luzhou area, southern Sichuan Basin, China. *J. Asian Earth Sci.* 263, 106025. doi:10.1016/j.jseaes.2024.106025

Fu, C. (2017). *Study on reservoir characteristics and shale gas enrichment of Wufeng-Longmaxi Formation shale in Southeast Chongqing*. China: China University of Mining and Technology.

Fu, Y. (2016). *Formation pressure prediction based on core data and seismic data*. Chengdu: Chengdu University of Technology. [master's thesis]. [Chengdu (Sichuan Province)].

Fu, Y., Jiang, Y., Dong, D., Hu, Q., Lei, Z., Peng, H., et al. (2021). Microscopic pore-fracture configuration and gas-filled mechanism of shale reservoirs in the western Chongqing area, Sichuan Basin, China. *Petroleum Explor. Dev.* 48 (5), 1063–1076. doi:10.1016/s1876-3804(21)60091-5

Fu, Y., Jiang, Y., Wang, Z., Hu, Q., Xie, J., Ni, G., et al. (2019). Non-connected pores of the Longmaxi shale in southern Sichuan Basin of China. *Mar. Petroleum Geol.* 110, 420–433. doi:10.1016/j.marpetgeo.2019.07.014

Gao, Y., Cai, X., He, X., Wu, Y., Ding, A., Gao, H., et al. (2020). Relationship between shale pressure system and organic pore development of Wufeng-Longmaxi Formation in marginnal conversion zone of Southeastern Chongqing Basin. *J. Jilin Univ. Earth Sci. Ed.* 50 (2), 662–674. doi:10.13278/j.cnki.jjuese.20190130

Gong, L., Liu, K., and Ju, W. (2023). Editorial: advances in the study of natural fractures in deep and unconventional reservoirs. *Front. Earth Sci.* 10, 1096643. doi:10.3389/feart.2022.1096643

Guo, T. (2016). Key geological issues and main controls on accumulation and enrichment of Chinese shale gas. *Petroleum Explor. Dev.* 43 (3), 349–359. doi:10.1016/s1876-3804(16)30042-8

Guo, W., Tang, J., Ouyang, J., Wang, T., Wang, X., and Wang, Y. (2021). Characteristics of structural deformation in the southern Sichuan Basin and its relationship with the storage condition of shale gas. *Nat. Gas. Ind.* 41 (5), 11–19. doi:10.3787/j.issn.1000-0976.2021.05.002

Hao, F., Zou, H., and Lu, Y. (2013). Mechanisms of shale gas storage:Implications for shale gas exploration in China. *AAPG Bull.* 97 (8), 1325–1346. doi:10.1306/02141312091

Hu, M., Huang, W., and Li, J. (2017). Effects of structural characteristics on the productivity of shale gas wells: a case study on the Jiaoshiba Block in the Fuling Shale gas field, Sichuan Basin. *Nat. Gas. Ind.* 37 (8), 31–39. doi:10.3787/j.issn.1000-0976.2017.08.004

Jiang, Y., Chen, L., Qi, L., Luo, M., Chen, X., Tao, Y., et al. (2017). Characterization of the lower silurian Longmaxi marine shale in changning area in the South Sichuan basin, China. *Geol. J.* 53, 1656–1664. doi:10.1002/gj.2983

Jiang, Y., Fu, Y., Lei, Z., Gu, Y., Qi, L., and Cao, Z. (2019). Experimental NMR analysis of oil and water imbibition during fracturing in Longmaxi shale, SE Sichuan Basin. *J. Jpn. Petroleum Inst.* 62 (1), 1–10. doi:10.1627/jpi.62.1

Jiang, Y., Song, Y., Qi, L., Chen, L., Tao, Y., Gan, H., et al. (2016). Fine lithofacies of China's marine shale and its logging prediction: a case study of the Lower Silurain Longmaxi marine shale in Weiyuan area, southern Sichuan Basin, China. *Earth Sci. Front.* 23 (1), 107–118. doi:10.13745/j.esf.2016.01.010

Jin, Z., Zhang, Q., Zhu, R., Dong, L., Fu, J., Liu, H., et al. (2023). Classification of lacustrine shale oil reservoirs in China and its significance. *Oil&Gas Geol.* 44 (4), 801–819. doi:10.11743/ogg20230401

Klaver, J., Desbois, G., Littke, R., and Urai, J. L. (2015). BIB-SEM characterization of pore space morphology and distribution in postmature to overmature samples from the Haynesville and Bossier Shales. *Mar. Petroleum Geol.* 59, 451–466. doi:10.1016/j.marpetgeo.2014.09.020

Ko, L. T., Ruppel, S. C., Loucks, R. G., Hackley, P. C., Zhang, T., and Shao, D. (2018). Pore-types and pore-network evolution in Upper Devonian-Lower Mississippian Woodford and Mississippian Barnett mudstones: insights from laboratory thermal maturation and organic petrology. *Int. J. Coal Geol.* 190, 3–28. doi:10.1016/j.coal.2017.10.001

Li, H. (2023a). Coordinated development of shale gas benefit exploitation and ecological environmental conservation in China: a mini review. *Front. Ecol. Evol.* 11, 1232395. doi:10.3389/fevo.2023.1232395

Li, H. (2023b). Deciphering the formation period and geological implications of shale tectonic fractures: a mini review and forward-looking perspectives. *Front. Energy Res.* 11, 1320366. doi:10.3389/fenrg.2023.1320366

Li, Z., Jiang, Z., Liang, Z., Yu, H., and Yang, Y. (2019). Pore-structure characterisation of tectonically deformed shales: a case study of Wufeng-Longmaxi Formation in western Hunan Province, southern China. *Aust. J. Earth Sci.* 66 (7), 1075–1084. doi:10.1080/08120099.2019.1588168

Liang, X., Xu, J., Wang, Y., Fang, X., Zhao, L., Wu, Y., et al. (2021). The shale gas enrichment factors of Longmaxi Formation under gradient basin-mountain boundary in South Sichuan Basin: tectono-depositional differentiation and discrepant evolution. *Chin. J. Geol.* 56 (1), 60–81. doi:10.12017/dzkx.2021.005

Liu, S., Ye, Y., Ran, B., Jiang, L., Li, Z., Li, J., et al. (2020). Evolution and implications of shale pore structure characteristics under different preservation conditions. *Reserv. Eval. Dev.* 10 (5), 1–11. doi:10.13809/j.cnki.cn32-1825/te.2020.05.001

Loucks, R. G., Reed, R. M., Ruppel, S. C., and Hammes, U. (2012). Spectrum of pore types and networks in mudrocks and a descriptive classification for matrix-related mudrock pores. *AAPG Bull.* 96 (6), 1071–1098. doi:10.1306/08171111061

Luo, C., Li, J., Li, Z., Zhang, D., Tong, K., Dai, Y., et al. (2022). Structural deformation characteristics and formation process of Luzhou block in Sichuan Basin, China. *J. Chengdu Univ. Technol. Sci. &.Technology Ed.* 49 (6), 665–673. doi:10.3969/j.issn.1671-9727.2022.06.03

Ma, X., Zeng, L., Tian, H., Shi, X., Wu, W., Yang, S., et al. (2023). Fault damage zone and its effect on deep shale gas: insights from 3D seismic interpretation in the southern Sichuan Basin, China. *J. Struct. Geol.* 170, 104848. doi:10.1016/j.jsg.2023.104848

Milliken, K. L., Rudnicki, M., Awwiller, D. N., and Zhang, T. (2013). Organic matter-hosted poresystem, marcellus formation (devonian), Pennsylvania. *AAPG Bull.* 97 (2), 177–200. doi:10.1306/07231212048

Pommer, M., and Milliken, K. (2015). Pore types and pore-size distributions across thermal maturity, Eagle Ford Formation, southern Texas. *AAPG Bull.* 99 (9), 1713–1744. doi:10.1306/03051514151

Qiu, N., Liu, Y., Liu, W., and Jia, J. (2020). Quantitative reconstruction of formation paleo-pressure in sedimentary basins and case studies. *Sci. China Earth Sci.* 63, 808–821. doi:10.1007/s11430-019-9556-8

Sing, K. S. W., Everett, D. H., Haul, R. A. W., Moscou, L., Pierotti, R. A., Rouquerol, J., et al. (1985). Reporting physisorption data for gas/solid systems with special reference to the determination of surface area and porosity (Recommendations 1984). *Pure Appl. Chem.* 57, 603–619. doi:10.1351/pac198557040603

Tang, J., Li, Y., Wang, K., and Qi, Z. (2015). Comprehensive evaluation of effective preservation zone of Longmaxi Formation shale gas in the Southeast Sichuan Basin. *Nat. Gas. Ind.* 35 (5), 15–23. doi:10.3787/j.issn.1000-0976.2015.05.003

Tang, L., Song, Y., Zhao, Z., Jiang, Z., Jiang, S., Chen, X., et al. (2022). Origin and evolution of overpressure in shale gas reservoirs of the upper ordovician Wufeng Formation-lower silurian Longmaxi Formation in the Sichuan Basin. *Nat. Gas. Ind.* 42 (10), 37–53. doi:10.3787/j.issn.1000-0976.2022.10.004

Tang, X. (2018). *Tectonic control of shale gas accumulation in Longmaxi Formation in the southern Sichuan Basin. [dissertation]. [Xuzhou (jiangsu province)]*. China: China University of Mining and Technology.

Thommes, M., Kaneko, K., Neimark, A. V., Olivier, J. P., Rodriguez-Reinoso, F., Rouquerol, J., et al. (2015). Physisorption of gases, with special reference to the evaluation of surface area and pore size distribution (IUPAC Technical Report). *Pure Appl. Chem.* 89 (9-10), 1051–1069. doi:10.1515/pac-2014-1117

Wang, H., Shi, Z., Zhao, Q., Liu, D., Sun, S., Guo, W., et al. (2020). Stratigraphic framework of the Wufeng-Longmaxi shale in and around the Sichuan Basin, China: implications for targeting shale gas. *Energy Geosci.* 1 (3-4), 124–133. doi:10.1016/j.engeos.2020.05.006

Wang, P. (2017). The correlation between shale sealing capacity and the gas generation characteristics of shale organic matter, minerals compositions and pore structure. *Univ. Chin. Acad. Sci*.

Wang, X. (2021).*Study on shale gas accumulation process and enrichment mechanism of Wufeng-Longmaxi Formation in Changning Area*. China: China University of Mining and Technology.

Wang, Z., Guo, B., Jiang, C., Qi, L., Jiang, Y., Gu, Y., et al. (2022). Nanoscale pore characteristics of the lower permian shanxi formation transitional facies shale, eastern ordos basin, North China. *Front. Earth Sci.* 10, 842955. doi:10.3389/feart.2022.842955

Wu, J., Chen, X., Liu, W., Wu, W., Gao, Y., Luo, C., et al. (2022). Fluid activity and pressure evolution process of Wufeng-Longmaxi shales, Southern Sichuan Basin. *Earth Sci.* 47 (2), 518–531. doi:10.3799/dqkx.2021.049

Xiang, J., Zhu, Y., Wang, Y., Chen, S., and Jiang, Z. (2022). Effect of faults on shale pore fracture and shale gas preservation: a case study of the Wufeng-Longmaxi Formation in the Northeast Yunnan Area. *Energy fuels.* 36, 8238–8255. doi:10.1021/acs.energyfuels.2c01834

Yang, H., Zhao, S., Liu, Y., Wu, W., Xia, Z., Wu, T., et al. (2019). Main controlling factors of enrichment and high-yield of deep shale gas in the Luzhou Block, southern Sichuan Basin. *Nat. Gas. Ind.* 39 (11), 55–63. doi:10.3787/j.issn.1000-0976.2019.11.007

Yang, R. (2018). *Pore structure and tracer-containing fluid migration in connected pores of Wufeng and Longmaxi shales from western Hubei and eastern Chongqing regions. [dissertation]. [Wuhan (Hubei Province)]*. Wuhan: China University of Geosciences.

Yang, W., Wang, Y., Du, W., Song, Y., Jiang, Z., Wang, Q., et al. (2022). Behavior of organic matter-hosted pores within shale gas reservoirs in response to differential tectonic deformation: potential mechanisms and innovative conceptual models. *J. Nat. Gas Sci. Eng.* 102 (2022), 104571. doi:10.1016/j.jngse.2022.104571

Yu, W., and Tang, H. (2019). Experimental study on the existence of nano-scale pores and the evolution of organic matter in organic-rich shale. *Nanotechnol. Rev.* 8, 156–167. doi:10.1515/ntrev-2019-0015

Zeng, L., Gong, L., Guan, C., Zhang, B., Wang, Q., Zeng, Q., et al. (2022). Natural fractures and their contribution to tight gas conglomerate reservoirs: a case study in the northwestern Sichuan Basin, China. *J. Petroleum Sci. Eng.* 210 (2022), 110028. doi:10.1016/j.petrol.2021.110028

Zeng, L., Gong, L., Zhang, Y., Dong, S., and Lyu, W. (2023). A review of the genesis, evolution, and prediction of natural fractures in deep tight sandstones of China. *AAPG Bull.* 107 (10), 1687–1721. doi:10.1306/07052322120

Zhang, C., Yao, Y., Elsworth, D., Liu, D., Ju, Y., Dong, Y., et al. (2021). Microstructure characterization of kerogen in mature shale: molecular investigation of micropore development. *J. Nat. Gas Sci. Eng.* 95, 104239. doi:10.1016/j.jngse.2021.104239

Zhang, K. (2019). *Preservation mechanism and evaluation method of marine shale gas with complex tectonic background*. Beijing: China University of Petroleum.

Zheng, S., Yao, Y., Elsworth, D., Wang, B., and Liu, Y. (2020). A novel pore size classification method of coals: investigation based on NMR relaxation. *J. Nat. Gas Sci. Eng.* 80, 103466. doi:10.1016/j.jngse.2020.103466

Zhou, S., Wang, H., Li, B., Li, S., Sepehrnoori, K., and Cai, J. (2022). Predicting adsorbed gas capacity of deep shales under high temperature and pressure: experiments

and modeling. *Adv. Geo-Energy Res.* 26 (6), 482–491. doi:10.46690/ager.2022.06.05

Zhou, Y., Wang, Z., Hu, D., Wei, Z., Wei, X., Liu, R., et al. (2023). Nanoscale pore characteristics of the jurassic dongyuemiao member lacustrine shale, eastern Sichuan Basin, SW China: insights from SEM, NMR, LTNA, and MICP experiments. *Front. Earth Sci.* 10, 1055541. doi:10.3389/feart.2022.1055541

Zhu, H., Ju, Y., Sun, Y., Huang, C., Feng, H., Raza, A., et al. (2021a). Evolution characteristics and models of shale pores and fractures under tectonic deformation: a case study of the Lower Paleozoic marine shale in the Sichuan Basin and its periphery. *Oil Gas Geol.* 42 (1), 186–200+240. doi:10.11743/ogg20210116

Zhu, Y., Chen, G., Liu, Y., Shi, X., Wu, W., Luo, C., et al. (2021b). Sequence stratigraphy and lithofacies paleogeographic evolution of katian stage-aeronian stage in southern Sichuan Basin, SW China. *Petroleum Explor. Dev.* 48 (5), 1126–1138. doi:10.1016/S1876-3804(21)60096-4

Zou, C., Dong, D., Wang, Y., Li, X., Huang, J., Wang, S., et al. (2016a). Shale gas in China: characteristics, challenges and prospects (II). *Petroleum Explor. Dev.* 43 (2), 182–196. doi:10.1016/s1876-3804(16)30022-2

Zou, C., Dong, D., Wang, Y., Li, X., Huang, J., Wang, S., et al. (2016b). Shale gas in China: characteristics, challenges and prospects (I). *Petroleum Explor. Dev.* 42 (6), 689–701. doi:10.11698/PED.2015.06.01